Chemical Engineering Journal 430 (2022) 133025

Contents lists available at ScienceDirect

Chemical Engineering Journal

journal homepage: www.elsevier.com/locate/cej

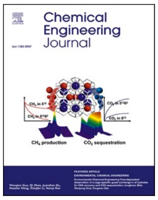

The decomplexation of Cu-EDTA by electro-assisted heterogeneous activation of persulfate via acceleration of Fe(II)/Fe(III) redox cycle on Fe-MOF catalyst

Yue Zhang [a,b,c], Jian Sun [a,*], Ziwei Guo [b,c], Xinqi Zheng [a,b,c], Pengran Guo [b,c], Jingwei Xu [b], Yongqian Lei [b,c,*]

[a] *Guangzhou Key Laboratory of Environmental Catalysis and Pollution Control, Guangdong Key Laboratory of Environmental Catalysis and Health Risk Control, School of Environmental Science and Engineering, Institute of Environmental Health and Pollution Control, Guangdong University of Technology, Guangzhou 510006, China*

[b] *Guangdong Provincial Key Laboratory of Emergency Test for Dangerous Chemicals, Institute of Analysis, Guangdong Academy of Sciences (China National Analytical Center, Guangzhou), Guangzhou 510070, China*

[c] *Guangdong Provincial Engineering Research Center for Online Monitoring of Water Pollution, Institute of Analysis, Guangdong Academy of Sciences (China National Analytical Center, Guangzhou), Guangzhou 510070, China*

ARTICLE INFO

Keywords:
Cu-EDTA
Ferreous metal-organic frameworks
Heterogeneous
Electrochemical
Persulfate

ABSTRACT

As a metal complex widely used in the electroplating industry, the degradation of Cu-EDTA in the wastewater treatment process is difficult for its strong stability, it is a crucial but extremely challenging task. In this study, a novel Ferreous metal–organic frameworks (Fe-MOF) heterogeneous catalyst was synthesized by a convenient and fast microwave method. Combined with electrochemical (EC) method and persulfate (PS), an EC/Fe-MOF/PS system was firstly applied to degrade the Cu-EDTA that was completely removed under the optimized conditions. During this process, the redox cycle was accelerated with electrical assistance and the ratio of Fe(II)/Fe(III) on the Fe-MOF was significantly increased, which improved the catalytic ability. Additionally, the degradation performance was obviously enhanced with the increased cycles. The phenomenon occurred because that Cu species derived from the decomposition of Cu-EDTA was deposited on Fe-MOF surface, and the additional catalytic ability was obtained from the Cu(0)/Cu(I)/Cu(II). The detailed pathway of Cu-EDTA degradation was proposed based on the intermediates identified by FT-ICR-MS and the mechanism was also investigated by Electron spin resonance (ESR) and quenching experiments of Reactive oxygen species (ROS). Furthermore, the EC/Fe-MOF/PS system could also represent excellent performance for the degradation of various metal-EDTA complexes. This study provided an efficient and sustainable approach for the degradation of refractory organic pollutants.

1. Introduction

With the development of industry, heavy metal pollution has become a global public concern because of its damage to human health and the ecological environment [1,2]. As a chelate of heavy metal and organic ligand, copper-ethylene diamine tetraacetic acid (Cu-EDTA) is widely present in effluent discharged from the process of acidification, rinsing and plating in the electroplating industry [3–6]. Because of the heterocyclic ring formed by central metal and coordination atom (three or four −COOH and two nitrogen atoms), the chelate is characteristically by its refractory biodegradability, high solubility, and strong stability [7,8].

Currently, different technologies that are mainly classified as non-destructive and destructive methods have been applied for the removal of metal-EDTA complexes. The non-destructive methods such as ion exchange, adsorption, and chemical precipitation [9–12] target the decrease of heavy metal content but hardly degrade EDTA that will recombine with other heavy metals in subsequent processing to form new complexes [13]. Comparatively, destructive methods such as Fenton, photocatalysis and other Advanced oxidation processes (AOP) can destroy organic ligands and remove EDTA fundamentally [14–18]. However, the performance of the photocatalytic system alone was poor due to the short distance of light penetration in wastewater [14]. The application of Fenton is also limited by the fact that (1) the additional separation and treatment of iron sludge generated by the homogeneous

---

* Corresponding authors.
E-mail addresses: sunjian472@163.com (J. Sun), yqlei@fenxi.com.cn (Y. Lei).

https://doi.org/10.1016/j.cej.2021.133025
Received 9 July 2021; Received in revised form 10 October 2021; Accepted 12 October 2021

system; (2) the heavy use of catalysts; (3) the high corrosion resistance requirements for the equipment because the Fenton was only applicable in a narrow acid pH range. At present, the sulfate-based advanced oxidation process (SR-AOP) has attracted widespread attention. Compared with hydroxyl radicals ($HO^{\bullet}$), the sulfate radical ($SO_4^{\bullet -}$) generated by persulfate (PS) is more reactive owing to higher redox potential ($E^0_{SO_4^{\bullet -}}$=2.50 ~ 3.10 V, $E^0_{HO^{\bullet}}$=1.90 ~ 2.70 V) as well as better mineralization ability due to wider pH application range and higher selectivity [19–23]. Many studies on PS have been published so far. Ghauch reported the PS oxidation systems that had higher reaction stoichiometric efficiency (RSE) than the H_2O_2 system [17,24–28]. In chemically activated PS system, the %RSE was less than 10% [29–31], which can be improved with MOF/PS system [32].

Ferreous metal-organic frameworks (Fe-MOFs) are considered as the promising heterogeneous catalyst in AOP due to their excellent features of adjustable pore size, high surface area and accessible unsaturated metal sites [33–36]. Previous studies have indicated that Fe-MOF, such as MIL-53(Fe) [37], MIL-88(A) [32,38], MIL-101(Fe) [36] can activate PS into strong oxidizing $SO_4^{\bullet -}$ via the conversion of Fe(II) and Fe(III) (Eq. (2)). However, with the consumption of Fe(II) on the Fe-MOF in the SR-AOP, the catalytic activity of Fe-MOF become weaker, which restricted its potential application as a heterogeneous catalyst. It was reported that Fe^{2+} could be regenerated from the reduction of Fe^{3+} at the cathode, at the same time, more $SO_4^{\bullet -}$ generated through electron transfer reaction, which improved the degradation efficiency [39,40]. Besides, the traditional synthesis method of MOF materials is time-consuming (the hydrothermal process takes 24 h), requires the addition of harmful solvent (DMF) and highly corrosive acid (HF) [41,42]. The development of convenient, rapid, green and economical synthesis methods of MOF is very important to further expand its scale and practical application. Compared with traditional hydrothermal method, the microwave method has the advantage of rapid heating of the reaction mass, the rapid cooling after switching off microwave power and high efficiency of the energy consumption [43].

Here we hypothesized that the combination of Fe-MOF heterogeneous catalyst with Electrochemical (EC) method and SR-AOP would have their advantages of wide pH range, high activity and cycle stability. In this study, a novel Fe-MOF catalyst was prepared by a simple and rapid microwave method using water as solvent. With the electro-assisted process, a heterogeneous catalytic system of EC/Fe-MOF/PS was firstly used to degrade M-EDTA (M=Cu, Ni, Pb, Cd) complexes. The different systems and the factors involve PS concentration, initial pH, current density, electrolyte concentration and catalyst dosage were optimized. The reusable performance of Fe-MOF catalyst was investigated and the possible mechanism and pathways for Cu-EDTA degradation were also proposed.

2. Materials and methods

2.1. Chemicals

All the chemicals and reagents were of analytical grade and used as received. More details of used chemicals and reagents can be found in Text S1 in the Supporting Information.

2.2. Experimental section

Fe-MOF was prepared by microwave method, $FeSO_4{\cdot}7H_2O$ (0.8 mmol) and H_3BTC (0.8 mmol) were ground in an agate mortar and place in NaOH (10 mL, 10 mM) solution [44]. After sonicating for 20 min, the mixed solution was transferred to a polytetrafluoroethylene (PTFE) reactor (50 mL) and moved to the microwave digestion system (TOPEX+, PreeKem) for microwave reaction with a specific microwave condition (temperature: 100 °C, 1 min; 150 °C, 1 min; 200 °C, 10 min. power: 668 w). The product (red-brown solid) was obtained after cooling at room temperature and washed three times with ethanol and deionized water, and then dried in a vacuum oven (70 °C, 12 h) for further use.

The electrochemical catalytic oxidation reaction was carried out in a 3D printed reactor (acrylonitrile-butadienestyrene copolymer, 6 cm × 7 cm × 7.5 cm), connecting to the direct current (DC) power, the graphite plates were used as the cathode and anode with a spacing of 6.5 cm. The aqueous solution of Cu-EDTA complex (1 mM, 100 mL) was mixed uniformly by magnetic stirring and added Na_2SO_4 (0 ~ 0.08 M) as the electrolyte. The initial pH of the Cu-EDTA solution was adjusted to 3 ~ 12 by H_2SO_4 (0.1 M) and NaOH (0.1 M). PS (0 ~ 8 mM) and Fe-MOF (0 ~ 1.2 g/L) were added to the reactor when the DC power (current density: 0 ~ 5.71 mA/m^2) was turned on. The samples were taken out from the reactor at a designated time interval and filtered through a 0.45 μm membrane for further analysis.

2.3. Analytical methods

2.3.1. Characterization of Fe-MOF heterogeneous catalyst

The ZEISS Sigma 300 Scanning electron microscope (SEM) was used to analyze the surface morphology of fresh and used Fe-MOF powder. The surface element composition and crystal structure of Fe-MOF were measured by an energy spectrometer (EDS, Smartedx) and the X-ray diffractometer (XRD, Bruker D8 advanced X-ray diffractometer) using Cu Kα radiation at a scan rate (2θ) of 0.2 °s^{-1}. The iron and copper on the surface of Fe-MOF were characterized by X-ray photoelectron spectroscopy (XPS, Thermo Scientific K-Alpha Nexsa) with Al Kα (1486.6 eV). The binding energies were calibrated with C1s=284.80 eV as standard. The structure information of the catalyst was also determined by Fourier Transform Infrared Spectroscopy (FTIR, Bruker VERTEX 70 & ALPHA) with the alkali halide (KBr) pressed pellet method. The surface area and porous structure of Fe-MOF were characterized by Brunauer-Emmett-Teller (BET, Micromeritics, ASAP2460) at 77 K.

2.3.2. Evaluation of the catalytic performance

The concentration of Cu-EDTA complexes was quantified by high-performance liquid chromatography (HPLC, 1260, Agilent Technology) with a C18 column (Agilent, 250 mm × 4.6 mm) and the ultraviolet detector (254 nm). The elution was comprised of water (80%, 0.02 mol/L tetrabutylammonium bromide and 0.03 mol/L sodium acetate buffer; adjusting pH=4.0 with phosphoric acid) and acetonitrile (20%). The flow rate was set as 0.8 mL/min. The residual proportion of Cu-EDTA was calculated by Eq. (1). The concentration of residual $S_2O_8^{2-}$ was measured by iodometry [45].

$$\text{Residual proportion} = \frac{C_{tCu-EDTA}}{C_{0Cu-EDTA}} \times 100\% \tag{1}$$

Where the $C_{t\text{-}Cu\text{-}EDTA}$ and $C_{0\text{-}Cu\text{-}EDTA}$ represented the concentration of Cu-EDTA in the solution at time and initial, respectively.

In the EC process, electrical energy consumption (EEC) is a consideration for commercial viability. Here, the following formula was used to estimate the energy consumption of the Cu-EDTA degradation (Eq. (2)).

$$\text{Electrical energy consumption}\left(\text{EEC}, \text{kWh/m}^3\right) = \frac{\text{UIt} \times 10^{-3}}{\text{V}} \tag{2}$$

Where the U, I, and t are applied voltage (V), current (A), and reaction time (h). V is the volume of reaction solution (m^3).

2.3.3. Investigation of the mechanism

The radicals in the water solution of various systems were identified by Electron spin resonance (ESR) experiments with the spectrometer (Bruker ELEXSYS-II E500 CW-EPR, Germany) using dimethyl pyridine N-oxide (DMPO) as the capture agent. Fourier-transform ion cyclotron resonance mass spectrometry (FT-ICR-MS, Bruker Solari X) was applied to identify intermediate products in process of electrochemical catalytic oxidation degradation.

3. Results and discussion

3.1. Characterization of Fe-MOF catalyst

As shown in Fig. 1a and 1b, the morphology of Fe-MOF was depicted a spindle-like shape with many cracks, which was similar to that of Fe (II)-MIL-53(Fe) and beneficial to the mass transfer of reactants according to the reference [37,46]. The XRD pattern showed that the prepared Fe-MOF represented a heterostructure (Fig. 1c). The characteristic peaks at 10.1°, 10.9° highly corresponded to the Fe-based MOFs reported [47–49]. The peak at 20.1° matched with H_3BTC and the remaining characteristic peaks were related to Hematite (Chemical Formula: Fe_2O_3, PDF#:99–0060) [50]. The functional groups of Fe-MOF were determined by FT-IR. The transmittance peaks of the fresh and used Fe-MOF (Fig. 1d) appeared at 3440 cm^{-1}, 1655 cm^{-1}, 1563 cm^{-1}, 1457 cm^{-1}, 1379 cm^{-1}, 750 cm^{-1}, 533 cm^{-1}. The broad peak at 3440 cm^{-1} was the O–H stretching vibration [51–53]. The three peaks at 1655 cm^{-1}, 1574 cm^{-1}, 1379 cm^{-1} were attributed to the stretching vibration as well as asymmetric and symmetric vibrations of C=O related groups, respectively, which confirmed the existence of free carboxyl groups and dicarboxylate linker within the sample [37,54]. The peak at 750 cm^{-1} was ascribed to C–H bending vibrations of the benzene. The apparent peak at 533 cm^{-1} was assigned to the stretching vibration of Fe-O that suggested the formation of iron-oxo clusters in prepared Fe-MOF [55]. Especially, the peak at 1457 cm^{-1} belonged to the antisymmetric bending vibration of RH [56,57] that was not mentioned in the literature, indicating the structure of this Fe-MOF was different from others, which was beneficial for the regeneration of Fe(II) as described in the following discussion. The BET test showed that the total pore volume and specific surface area of the fresh Fe-MOF were 0.3317 cm^3g^{-1} and 486.44 m^2g^{-1}, and both of them showed no significant changes after the reaction, which was 0.3391 cm^3g^{-1} and 514.98 m^2g^{-1}, respectively. The adsorption-desorption isotherm of N_2 (Fig.S1) showed an intermediate mode between type I and type Ⅳ, which suggested that the pore structure of the Fe-MOF was both mesoporous and microporous. The characterization results of the fresh and used Fe-MOF by SEM, XRD, FT-IR and BET indicated the insignificance effect on the Fe-MOF structure from the reaction.

3.2. Degradation of Cu-EDTA complex by different systems

Various contrast experiments of PS alone, Fe-MOF alone, MOF/PS, EC alone, EC/PS and EC/Fe-MOF/PS were applied to explore the degradation efficiency of Cu-EDTA and the consumption of PS. The results from Fig. 2a showed that there was almost no Cu-EDTA removal with PS alone (2.87%) and the PS remained 96.33% at 100 min, which indicated PS was stable at room temperature. MOFs were reported to adsorb plenty of organic pollutants [58,59], so the adsorption process on the prepared Fe-MOF should occur. However, the adsorption performance of Fe-MOF (Fe-MOF alone) on Cu-EDTA was not obvious (92.37% remained at 100 min). Comparatively, the concentration of Cu-EDTA was decreased to 41.47% at 40 min with the existence of both PS and Fe-MOF where the strong oxidizing radicals were generated by the reaction between Fe(II) and PS (Eq. (3)). The concentration decreased slightly after 40 min due to the exhaustion of the Fe(II) that was difficult to be regenerated in this system [60]. In the EC alone process, there was 36.77% Cu-EDTA residual when the reaction proceeded to 100 min, and the rate constant (k_1) of pseudo-first-order reaction kinetics was 1.08×10^{-2} min^{-1}. The electrochemical oxidation would generate hydroxyl radical ($HO^{\bullet}$) on the anode surface via Eq. (4) [61] and direct electron

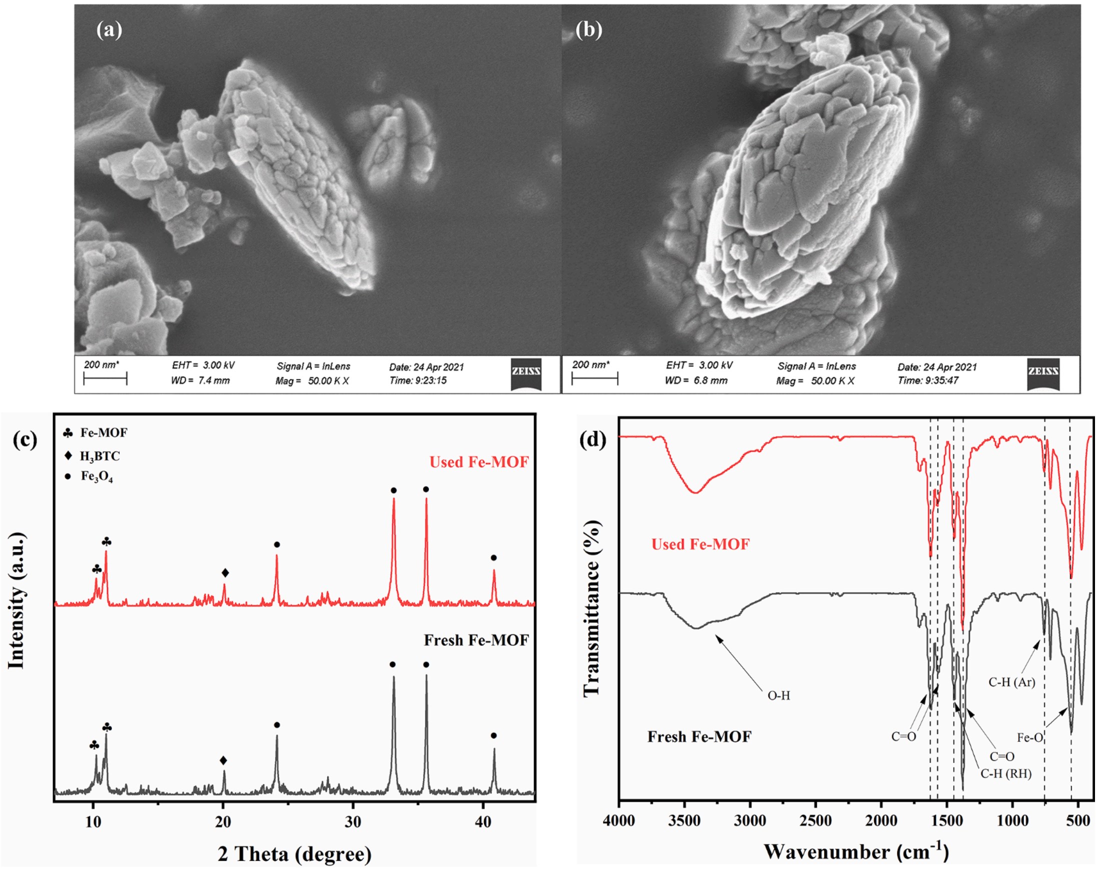

Fig.1. (a) SEM images of fresh Fe-MOF and (b) used Fe-MOF; (c) XRD patterns spectra of fresh and used Fe-MOF; (d) FTIR spectra of fresh and used Fe-MOF.

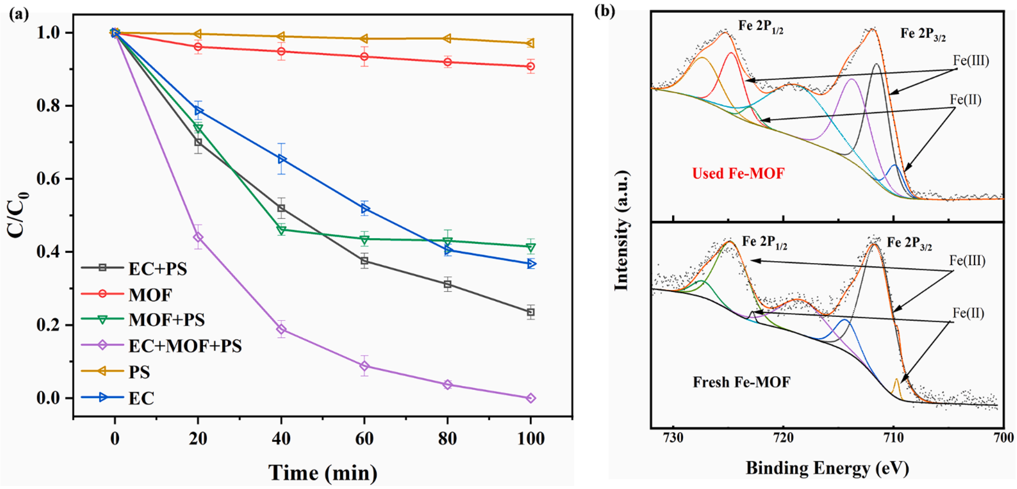

Fig. 2. (a) The effect on Cu-EDTA degradation and PS consumption of various systems (PS, Fe-MOF, Fe-MOF/PS, EC, EC/PS, EC/Fe-MOF/PS). Reaction conditions: [Fe-MOF] = 0.4 g/L, [PS] = 4 mM, $pH_0 = 3$, $[Cu\text{-}EDTA]_0 = 1$ mM, $[Na_2SO_4] = 0.02$ M, current density = 2.86 mA/cm^2, T = 25 °C; (b) Fe 2p XPS spectra of fresh and used Fe-MOF.

transfer (DET) also occurred [62–64]. The participation of PS to EC process made the remained Cu-EDTA decline to 23.50% with the rate constant up to 1.57×10^{-2} min^{-1}, this improvement of the degradation efficiency was attributed to the generation of $SO_4^{\bullet-}$ and $HO^{\bullet}$ (Eqs. (5)–(7)).

$$\equiv \mathrm{Fe(II)} + S_2O_8^{2-} \rightarrow \equiv \mathrm{Fe(III)} + SO_4^{\bullet-} + SO_4^{2-} \tag{3}$$

$$H_2O \rightarrow HO^{\bullet} + H^{+} + e^{-} \tag{4}$$

$$S_2O_8^{2-} + e^{-} \rightarrow SO_4^{\bullet-} + SO_4^{2-} \tag{5}$$

$$SO_4^{\bullet-} + H_2O \rightarrow SO_4^{2-} + HO^{\bullet} + H^{+} \tag{6}$$

$$SO_4^{\bullet-} + OH^{-} \rightarrow SO_4^{2-} + HO^{\bullet} \tag{7}$$

When the electric current was applied to the system of Fe-MOF/PS, the residual concentration of Cu-EDTA was decreased to 8.83% at 60

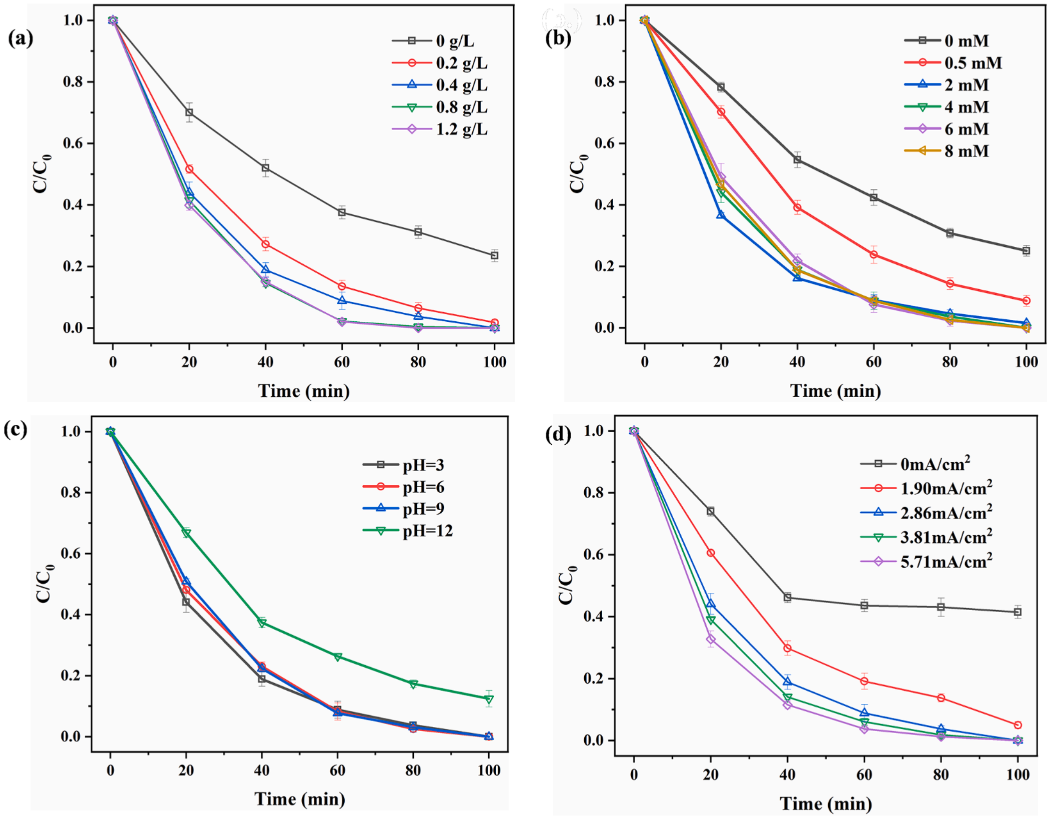

Fig. 3. Influences of Cu-EDTA degradation by several operating parameters. Reaction conditions: [Fe-MOF] = 0.4 g/L, [PS] = 4 mM, $pH_0 = 3$, $[Cu\text{-}EDTA]_0 = 1$ mM, $[Na_2SO_4] = 0.02$ M, current density = 2.86 mA/cm^2, T = 25 °C. Effect of crucial parameters, including (a) catalyst dosage, (b) PS concentration, (c) initial pH value and (d) current density on Cu-EDTA degradation in the EC/Fe-MOF/PS system.

min and it was completely degraded at 100 min. The rate constant (k_1) was 4.15 × 10^{-2} min^{-1}, which was the highest in all the systems and the best fitted with pseudo-first-order reaction kinetics. Meanwhile, the remaining PS in Fe-MOF/PS and EC/Fe-MOF/PS was 42.21% and 7.13% respectively, and their %RSE was higher than other PS oxidation systems with iron-based catalyst [29] and MOF catalyst [32] (Fig. S10). It can be inferred that in the EC/Fe-MOF/PS process, the Fe(II) was continuously regenerated by the reduction of Fe(III) at the cathode (Eq. (7)) and more $SO_4^{\bullet -}$ would be generated by PS via Eq. (3). To further verify the conversion of Fe(III) to Fe(II) in the EC/Fe-MOF/PS process, XPS was used to characterize the fresh Fe-MOF and used Fe-MOF (Fig. 2b). As illustrated in Table. S1, the ratio of Fe(II)/Fe(III) increased from 0.003 (fresh Fe-MOF) to 0.121 (used Fe-MOF), which suggested that more Fe(II) was regenerated on the surface of Fe-MOF by electrochemical reaction (Eq. (8)).

$$\equiv Fe(III) + e^- \rightarrow \equiv Fe(II) \tag{8}$$

3.3. Influences of operating parameters

3.3.1. Catalyst dosage

Fig. 3a illustrated that the degradation efficiency of Cu-EDTA with the catalyst dosage. In the absence of Fe-MOF, the residual Cu-EDTA was 23.5% and that was zero with the addition of 0.2 g/L catalysts at 100 min. The results showed that the degradation rate of Cu-EDTA had a remarkable growth with the increase of catalyst dosage at low concentration, but it became flat with more dosage addition. During the catalytic reaction, the Fe(II) reactive sites depended on the catalyst dosage, which was beneficial to the generation of $SO_4^{\bullet -}$ and $HO^\bullet$ via Eqs. (3) (6) (7) and enhanced the degradation of Cu-EDTA. However, excessive Fe-MOF could react with $HO^\bullet$ and SO_4^{2-} (Eqs. (9)-(10)), which resulted in the extra consumption of PS and Fe(II) [62,65] and the decrease in %RSE [29]. Considering the effective utilization, 0.4 g/L Fe-MOF was applied in the following experiments.

$$HO^\bullet + \equiv Fe(II) \rightarrow OH^- + \equiv Fe(III) \tag{9}$$

$$SO_4^{\bullet -} + \equiv Fe(II) \rightarrow SO_4^{2-} + \equiv Fe(III) \tag{10}$$

3.3.2. PS concentration

As the source of $SO_4^{\bullet -}$ in the EC/Fe-MOF/PS system, PS concentration is an important factor affecting the degradation efficiency of Cu-EDTA. In the absence of PS, the concentration of Cu-EDTA remained 25.04% with the rate constants of 1.42 × 10^{-2} min^{-1} at 100 min (Fig. 3b). The sightly addition of 0.5 mM PS made the remaining Cu-EDTA declined to 8.82% and the rate constant was 2.28 × 10^{-2} min^{-1}. With the addition of 2 mM PS, the remaining was decreased to 1.57% at 100 min even the rate constant was up to 4.68 × 10^{-2} min^{-1}, while Cu-EDTA was completely degraded in 4 mM PS with the constant rate of 4.15 × 10^{-2} min^{-1}. Further increasing the concentration of PS, the variation of the removal efficiency and the rate constant was insignificant. PS generated $SO_4^{\bullet -}$ by reacting with Fe(II) on Fe-MOF or directly activated at the cathode. Furthermore, PS also acted as the electrolyte in the aqueous solution and increased the rate of electron transfer. Therefore, the more PS concentration, the better degradation rate of Cu-EDTA was obtained. However, the excessive PS reacted with the sulfate radical (Eq. (11)) and radical self-combination also occurred (Eq. (12)), which decreased the utilization of oxidant and degradation efficiency of Cu-EDTA. Therefore, the PS concentration of 4 mM was considered as the most optimal concentration with %RSE of 27.2%, which was higher than other systems of MOF activated PS [32] and other technology of Cu-EDTA degradation. [17,66–68].

$$SO_4^{\bullet -} + S_2O_8^{2-} \rightarrow SO_4^{2-} + S_2O_8^{\bullet -} \tag{11}$$

$$SO_4^{\bullet -} + SO_4^{\bullet -} \rightarrow 2SO_4^{2-} \tag{12}$$

3.3.3. Effect of initial pH

The pH value was another key factor in the catalytic reaction, in here the initial pH of Cu-EDTA solution was adjusted to 3, 6, 9 and 12 before reaction. The degradation efficiency of Cu-EDTA decreased slightly when pH increased from 3 to 9 with rate constants of 4.15 × 10^{-2} min^{-1} and 3.73 × 10^{-2} min^{-1}, respectively. An apparent degression was observed when the pH = 12 and the rate constant decreased to 2.22 × 10^{-2} min^{-1} (Fig. 3c). The solution pH tended to decrease during the reaction process and the final solution was acidic (about 3) even at a high initial pH. It was reported [69,70] that the reaction of $SO_4^{\bullet -}$with $HO^\bullet$ or H_2O would release H^+ or consume OH^- (Eqs. (6)-(7)). And the H^+ was also released through the dissociation of HSO_4^-, which was produced by the decomposition of PS in H_2O or the reaction between $SO_4^{\bullet -}$ and $HO^\bullet$ (Eqs. (13)–(15)) The dissociation of HSO_4^- more easily occurred under alkaline conditions, which resulted in the extra consumption of $SO_4^{\bullet -}$ and $HO^\bullet$ radicals [63,71]. Normally the lower initial pH was more beneficial for the degradation. However, the effect of initial pH in this EC/Fe-MOF/PS system was insignificant and it could be applied within a wide range of pH.

$$SO_4^{\bullet -} + HO^\bullet \rightarrow HSO_4^- + \frac{1}{2}O_2 \tag{13}$$

$$S_2O_8^{2-} + H_2O \rightarrow 2HSO_4^- + \frac{1}{2}O_2 \tag{14}$$

$$HSO_4^- \rightarrow SO_4^{2-} + H^+ \tag{15}$$

3.3.4. Current density

As a significant factor of the degradation efficiency and running cost, the current density was optimized within the range of 0 ~ 5.71 mA/cm^2. The results in Fig. 3d showed that when the current density of 1.9 mA/cm^2 was applied to the Fe-MOF/PS system, the degradation rate of Cu-EDTA was improved obviously. The residual of Cu-EDTA declined from 41.5% to 4.97% with the rate constants of 1.24 × 10^{-2} min^{-1} and 2.75 × 10^{-2} min^{-1}, respectively. When the current density increased to 2.86 mA/cm^2, the Cu-EDTA was completely degraded with the rate constants of 4.15 × 10^{-2} min^{-1}. While the further increase of current density relieved the upward trend of degradation rate, the rate constant rose to 5.53 × 10^{-2} min^{-1} with the current density of 5.71 mA/cm^2. With the increase of current density, more hydroxyl radicals were formed on the surface of the anode (Eq. (4)) and more Fe(III) was reduced to Fe(II) at the cathode (Eq. (8)) that results in more generation of $SO_4^{\bullet -}$ (Eq. (3)). However, hydrogen would escape from the cathode via Eq. (16) with the current density further addition, which weakened the increase of degradation rate. Consequently, the optimal current density of 2.86 mA/cm^2 was used in the system for energy saving and high efficiency. The 7.58 kWh/m^3 of energy consumption was calculated by Eq. (3).

$$2H_2O + 2e^- \rightarrow H_2 + 2OH^- \tag{16}$$

3.4. Reusable performance of Fe-MOF catalyst

To investigate the reusable performance of Fe-MOF, the recycle experiments were carried out with the consistency of the experimental conditions and the results were shown in Fig. 4a. Interestingly, the removal efficiency was improved obviously with the increased cycles. By the 5th time of reaction, the removal rate of Cu-EDTA at 20 min was even higher than that at 40 min in the 1st run. Both of the removal rates in the 4th and 5th runs were reached 100% at 80 min. Apparently, the degradation rate constants were also accelerated with the growing of

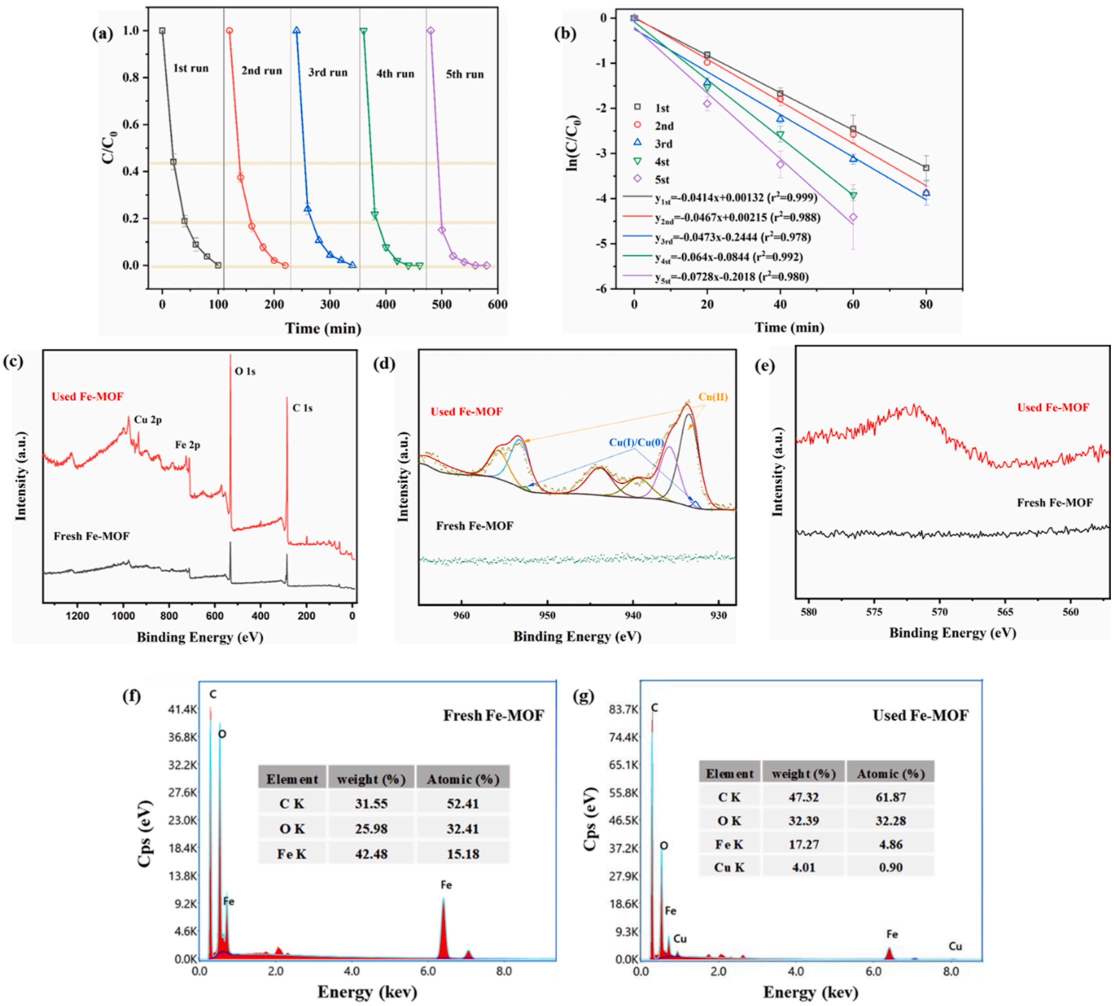

Element	weight (%)	Atomic (%)
C K	31.55	52.41
O K	25.98	32.41
Fe K	42.48	15.18

Element	weight (%)	Atomic (%)
C K	47.32	61.87
O K	32.39	32.28
Fe K	17.27	4.86
Cu K	4.01	0.90

Fig. 4. (a) Cu-EDTA degradation and (b) the kinetics in successive cycles. Reaction conditions: [Fe-MOF] = 0.4 g/L, [PS] = 4 mM, pH_0 = 3, $[Cu\text{-}EDTA]_0$ = 1 mM, $[Na_2SO_4]$ = 0.02 M, current density = 2.86 mA/cm^2, T = 25 °C; XPS spectra of fresh and used Fe-MOF (c) XPS survey, (d) Cu 2p and (e) Cu LM2; EDS of (f) fresh Fe-MOF and (g) used Fe-MOF.

cycles, which increased from 4.15×10^{-2} min^{-1} to 7.28×10^{-2} min^{-1} (Fig. 4b). Considering that the graphite electrode as the cathode may be coated with copper by the reduction of the free Cu ion in the solution [72], a new or absolutely cleaned graphite plate was used as the electrode in each recycle experiment. Therefore, the main influence factor for the removal efficiency should come from the variation on the Fe-MOF after several recycles.

Previous studies [73–77] showed that metal oxides often acted as effective catalysts in AOP or improved the performance of catalysts by doping. For example, the CuO was used to activate PS and generate radicals for the degradation of phenol [74]. Herein, considering the catalytic effect of Cu species, the following hypothesis was proposed: in the process of degradation, part of the generated free Cu ions was reduced on the cathode, while some of Cu ions deposited on the surface of Fe-MOF to form Cu(0)/Cu(I)/Cu(II) layer, which could also activated PS [75,78,79]. Therefore, with the recycle number increasing, Cu(0)/Cu (I)/Cu(II) layer on the Fe-MOF was piled up, and the catalytic performance of Fe-MOF was greatly improved.

To confirm this hypothesis, XPS and EDS were used to characterize the fresh and used Fe-MOF. The XPS survey showed that (Fig. 4c) there were no peaks in the range of Cu2p and CuLM2 in fresh-Fe-MOF, while the distinct peaks appeared in the used Fe-MOF. The fine scanning spectrum of Cu2p showed that there were two peaks at 933.1 eV and 932.7 eV, which were corresponding to Cu(II) and Cu(I)/Cu(0) [80]. It was speculated that the activation of PS may be accelerated by the cycling of Cu(0)/Cu(I)/Cu(II) couple formed on Fe-MOF via Eq. (17). Besides, through the EDS elemental analysis, Cu was detected on the used Fe-MOF (Fig. 4g), which also indicated that Cu species were deposited on Fe-MOF.

$$S_2O_8^{2-} + Cu^{+} \rightarrow SO_4^{\cdot -} + SO_4^{2-} + Cu^{2+} \qquad (17)$$

3.5. The degradation pathway of Cu-EDTA

In order to explore the decomplexation pathway of Cu-EDTA in the EC/PS/Fe-MOF process, the evolution of the HPLC spectra during the degradation process was analyzed. It was seen from Fig. S3 that there was an apparent peak corresponding to the Cu-EDTA at about 11 min (Fig. S3a). As the reaction conducted, the peak area of Cu-EDTA decreased gradually, and peaks of the byproducts were also varied constantly. According to the various retention times (RTs) [14], the possible intermediate products were Cu-ED3A, Cu-ED2A and Cu-EDMA, etc. For further identification, FT-ICR-MS was used to analyze the decomplexation products. As exhibited in Fig. S5, the mass spectra peaks (m/z) at 351.996, 293.991, 250.994, 235.007, 214.894 and 192.941 appeared with copper isotope peaks corresponded to Cu-EDTA, Cu-ED3A, Cu-NTA, Cu-ED2A, Cu-EDMA and Cu-IDA, respectively. Previous studies showed that C—C and C—N bonds were relatively easy to be broken in Cu-EDTA [81]. Xu et al. reported that the oxidative decomposition of Cu-EDTA was approximately a continuous decarboxylation process [17]. Herein, a possible degradation pathway of Cu-EDTA in this system was proposed (Fig. 5). The degradation of Cu-EDTA may occur by the carboxyl pathway (1) and amino pathway (4). For the carboxyl pathway, the C—N bond of one terminal -N-(CH_2-COOH)$_2$ group in Cu-EDTA was cleaved firstly and an acetic was removed, leading to the formation of Cu-ED3A. Secondly, Cu-ED2A and Cu-EDMA were degraded by repeating the process (1). For amino pathway, the C-N bond of Cu-EDTA was cleaved in -N-CH_2-CH_2- group with an iminodiacetic acid broken off and rapidly oxidized to Cu-NTA by $HO_2^{\bullet}$, which generated from H_2O_2 in solution (Eqs. (18)-(19)) [82–84]. And then the carboxyl group was removed to form Cu-IDA. Eventually, these intermediates were further decompressed into low molecules and inorganic substances.

$$HO^{\bullet} + HO^{\bullet} \rightarrow H_2O_2 \tag{18}$$

$$Cu^{2+} + H_2O_2 \rightarrow Cu^{+} + HO^{\bullet}_2 + H^{+} \tag{19}$$

3.6. Proposed reaction mechanism

To investigate the degradation mechanism in EC/Fe-MOF/PS system, Electron spin resonance (ESR) experiments were performed at the reaction time of 5 min, 10 min and 20 min. In parallel, both systems of Fe-MOF/PS and Fe-MOF/EC at the reaction time of 5 min were also explored. Matlab software was used to fitting peaks for the experimental data, which were shown and marked in Fig. 6 (the fitting details were shown in Fig. S5). Within the reaction time of 20 min, the peaks of DMPO-OH and DMPO-R were detected in the EC/Fe-MOF/PS system. Besides, there were trivial peaks of DMPO- R^1R^2NO and DMPO-H (Fig. S5) within the shorter time (5 min and 10 min), which were derived from the oxidation of DMPO and the electrolysis of water or metal catalytic reaction, respectively [85]. It could be seen that (Fig. 6a) the species and concentration of radical decreased with the reaction time. Fig. 6.b indicated that the radical species existed in Fe-MOF/PS and Fe-MOF/EC systems. The signal of DMPO-H, DMPO-R, DMPO-R^1R^2NO and DMPO-OH were clearly detected in Fe-MOF/PS system. Comparatively, the former three also presented in the Fe-MOF/EC system, while the signal of DMPO-OH was not detectable due to the low concentration or absence possibly. In addition, by comparing the free radical species in Fe-MOF/PS and EC/Fe-MOF/PS system, it was found that the concentration of $HO^{\bullet}$ increased significantly with electrical assistance, which intuitively shows that the application of electricity was beneficial to the generation of reactive oxygen species.

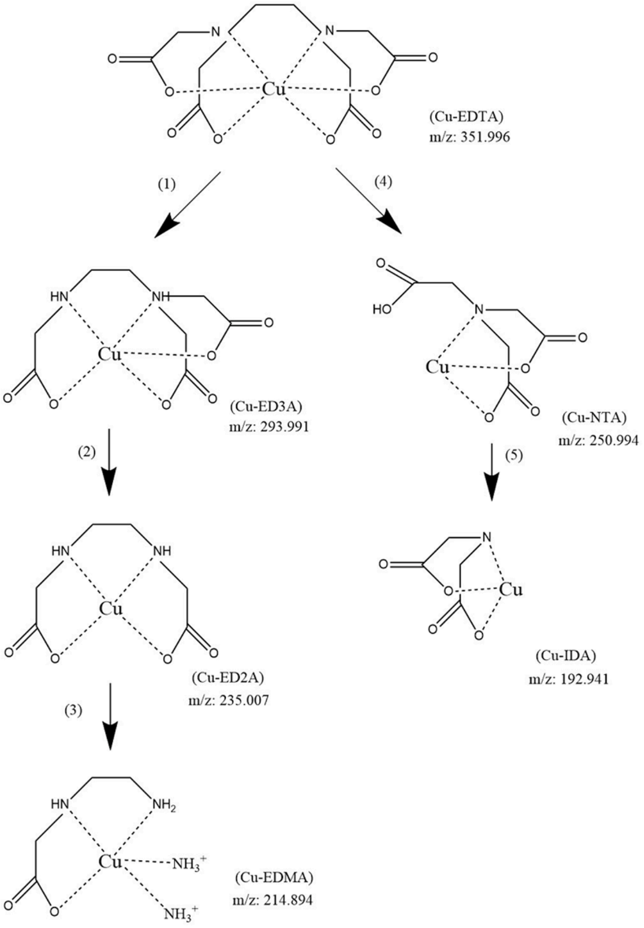

Fig. 5. Proposed reaction pathways for Cu-EDTA degradation in EC/Fe-MOF/PS system.

Despite the addition of PS, no signal of DMPO-SO_4^- was observed in all the systems. As the controlled experiments, the appearance of DMPO-OH signals in Fe-MOF/PS may be evolved from the evolution of $SO_4^{\bullet-}$ [86]. Particularly, $SO_4^{\bullet-}$ was generated from the reaction between PS and Fe-MOF (Eq. (3)), and react with H_2O or OH^- (Eqs. (6)-(7)) to produce $HO^{\bullet}$. Consequently, it was conjectured that the lack of DMPO-SO_4^- signal was resulted from the rapid conversion process of the unstable DMPO-SO_4^- to DMPO-OH by nucleophilic substitution reaction (Eq. (20)) [21,87]. The emergence of $R^{\bullet}$ in the system may be derived from the reaction of alkyl (RH) with $HO^{\bullet}$ via Eq. (21) [88]. It should be noted that the presence of RH in the prepared Fe-MOF was found by the FTIR experiment, which was rarely mentioned in the previous literature. Based on this, the viewpoint was proposed that the alkyl groups on Fe-MOF react with $HO^{\bullet}$ to generate $R^{\bullet}$ Fortunately, the Fe(II) could be regenerated faster by $R^{\bullet}$ (Eq. (22)) [89], which improved the degradation efficiency of Cu-EDTA. Furthermore, the superoxide radical and single oxygen in the system was also determined by ESR. No peaks were observed with capturing agents of TEMP in water as well as DMPO in methanol, which indicated that the absence of singlet oxygen and superoxide radical.

$$DMPO + SO_4^{-\bullet} \rightarrow DMPO - SO_4^{-} \rightarrow DMPO - OH \tag{20}$$

$$HO^{\bullet} + RH \rightarrow R^{\bullet} + H_2O \tag{21}$$

$$\equiv Fe(III) + R^{\bullet} \rightarrow \equiv Fe(II) + R^{+} \tag{22}$$

Generally, the *tert*-butanol (TBA) mainly scavenges $HO^{\bullet}$ instead of $SO_4^{\bullet-}$($k_{SO_4^{\bullet-}}, TBA = (4.0–9.1) \times 10^5$ $M^{-1}s^{-1}$, $k_{HO\cdot,TBA} = (3.8–7.6) \times 10^8$ $M^{-1}s^{-1}$), while isopropanol (IPA) and methanol (MeOH) have better quenching property for both $SO_4^{\bullet-}$ and $HO^{\bullet}$ ($k_{SO_4^{\bullet-}}, IPA = (6.0–8.2) \times 10^7$ $M^{-1}s^{-1}$, $k_{HO\cdot,IPA} = (1.9–2.8) \times 10^9$ $M^{-1}s^{-1}$; ($k_{SO_4^{\bullet-}}, MeOH = 3.2 \times 10^6$ $M^{-1}s^{-1}$,$k_{HO\cdot,MeOH} = 9.7 \times 10^8$ $M^{-1}s^{-1}$) [62]. The radical quenching experiment was carried out to investigate the contribution of $SO_4^{\bullet-}$ and $HO^{\bullet}$ of EC/Fe-MOF/PS system for the degradation of Cu-EDTA with the existence of IPA or TBA. As shown in Fig. 6c, with the addition of 1 M TBA, MeOH and IPA, the remaining Cu-EDTA was 5.84%, 24.59% and 31.7% at 100 min. The corresponding rate constants were 2.50×10^{-2} min^{-1}, 1.44×10^{-2} min^{-1} and 1.08×10^{-2} min^{-1}, which were far less than 4.15×10^{-2} min^{-1} without scavenger existence, revealing that $HO^{\bullet}$ and $SO_4^{\bullet-}$ existed in the system and participated in the degradation of Cu-EDTA.

As a result, the Cu-EDTA degradation procedure in EC/Fe-MOF/PS system was described in Fig. 7. Firstly, PS was activated by Fe(II) on Fe-MOF to generate $SO_4^{\bullet-}$ and Fe(III) (1), while Fe(II) would be reproduced via the reduction at cathodic and R• that derived from RH in Fe-MOF (2). The $SO_4^{\bullet-}$ generated HO• (3). Besides, $HO^{\bullet}$ and $SO_4^{\bullet-}$ were obtained at the anode and cathode respectively with electrical assistance (4) and (5). The reactive oxygen species (ROS) generated in EC/Fe-

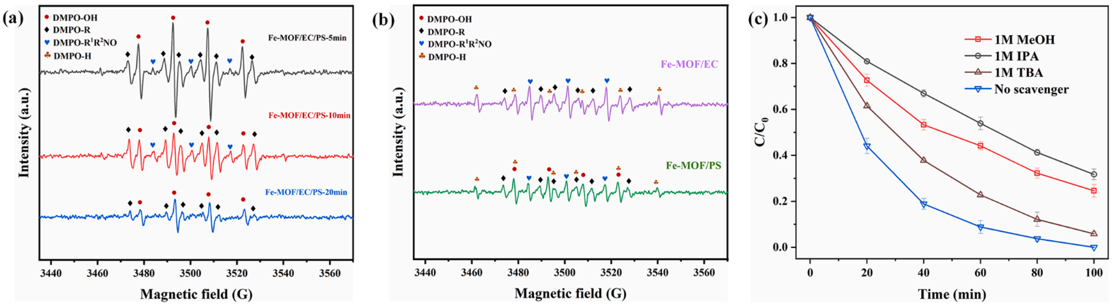

Fig. 6. EPR spectrum recorded at (a) different reaction times and (b) systems; (c) Effect of radical scavengers on the degradation of Cu-EDTA. Reaction conditions: [Fe-MOF] = 0.4 g/L, [PS] = 4 mM, pH_0 = 3, $[Cu\text{-}EDTA]_0$ = 1 mM, $[Na_2SO_4]$ = 0.02 M, current density = 2.86 mA/cm^2, T = 25 °C.

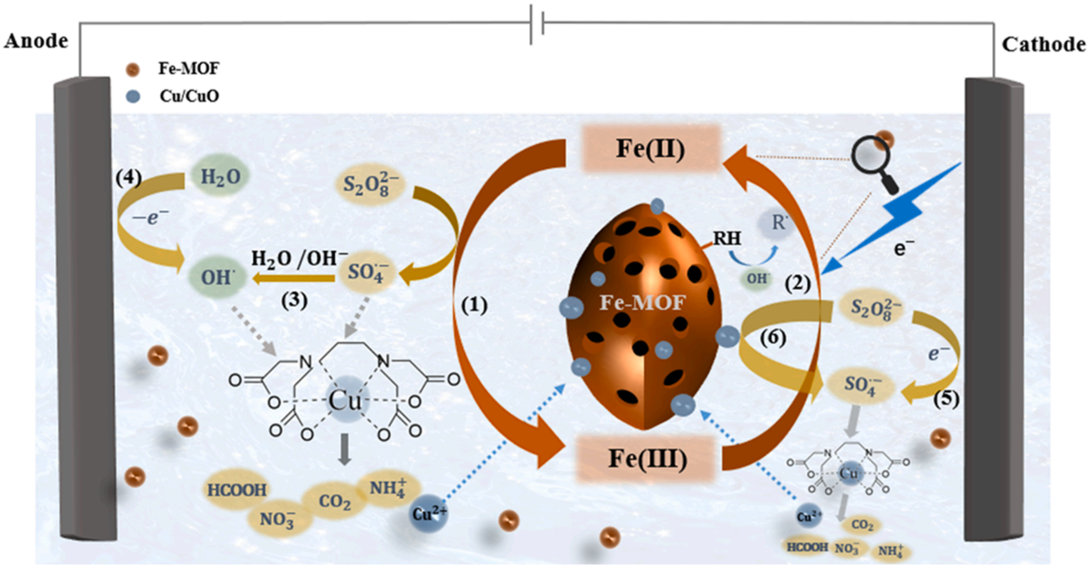

Fig. 7. Proposed mechanism of Cu-EDTA degradation by EC/Fe-MOF/PS system.

MOF/PS system and made Cu-EDTA transfer into free copper ions, low molecules and inorganic substances through the gradual decarboxylation/deamination process. The free copper ions deposited on the surface of Fe-MOF to form Cu(0)/Cu(I)/Cu(II) layer, which synergistically resulted in the generation of ROS for the degradation of Cu-EDTA (6).

3.7. Degradation performance on other heavy metal EDTA complexes

Furthermore, various metal-EDTA complexes including Ni-EDTA, Pb-EDTA, Cd-EDTA were used to evaluate the applicability of the EC/Fe-MOF/PS system. As shown in Fig. 8, these metals-EDTA complexes were completely removed at 100 min with the coincident condition of current density, initial concentration of metal complexes, pH, catalyst dose, PS and Na_2SO_4 concentration, which suggested that the system of EC/Fe-MOF/PS could be widely applied for the degradation of various metal complexes.

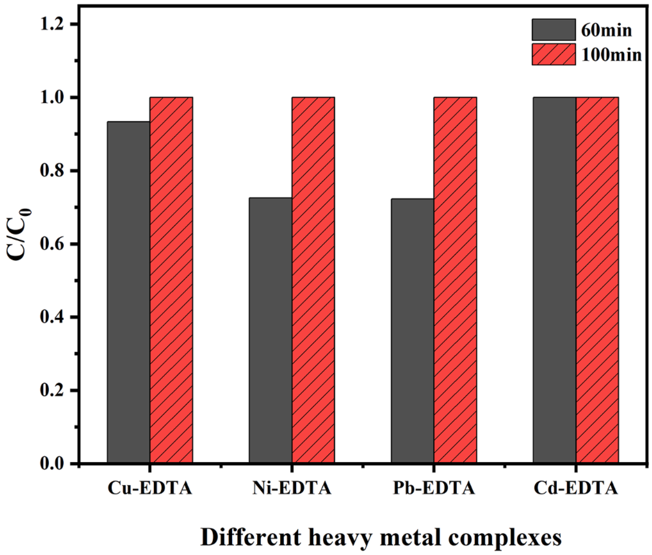

Fig. 8. The removal efficiency of other metal complexes. Reaction conditions: [Fe-MOF] = 0.4 g/L, [PS] = 4 mM, pH_0 = 3, $[Metal\text{-}EDTA]_0$ = 1 mM, $[Na_2SO_4]$ = 0.02 M, current density = 2.86 mA/cm^2, T = 25 °C.

4. Conclusions

In this study, a novel Fe-MOF catalyst with high surface area and accessible unsaturated sites was prepared with the convenient and fast microwave method. Combination with electrochemistry and PS, an EC/Fe-MOF/PS system was applied to degrade the Cu-EDTA complex. The Fe(II) on Fe-MOF could be persistently regenerated by the reduction of Fe(III) on the cathode with the assistance of electricity, which improved the utilization of the catalyst. The Cu-EDTA was completely degrade at 100 min and %RSE of 27.2% with the optimized conditions of initial pH

3.0, 1 mM Cu-EDTA, 4 mM PS, 0.4 g/L Fe-MOF, 0.02 M Na_2SO_4 and 2.86 mA/cm^2 current density. The reusable of this system was investigated. Surprisingly, the removal efficiency was obviously enhanced with the increase of the recycle times, which resulted from the Cu species deposited on Fe-MOF surface and more catalytic ability was obtained from the formation of Cu(0)/Cu(I)/Cu(II) layer. ESR and quenching experiments confirmed that the $SO_4^{\bullet-}$ and $HO^{\bullet}$ played important roles. Both gradual decarboxylation and deamination processes were proposed as Cu-EDTA decomposition pathways by FT-ICR-MS results. Moreover, various metal-EDTA complexes including Ni-EDTA, Pb-EDTA, and Cd-EDTA could also be degraded totally.

Declaration of Competing Interest

The authors declare that they have no known competing financial interests or personal relationships that could have appeared to influence the work reported in this paper.

Acknowledgments

This work was supported by National Natural Science Foundation of China (No. 21777150 and No. 51108186), Guangdong Provincial Key R&D Programm (2020B1111350002), and the Guangdong Special Support Program for Training High Level Talents, China (2015TQ01Z039). Thanks to Dr. Yuqi, Liu, South University of Science and Technology of China for the help on Matlab program.

Appendix A. Supplementary data

Supplementary data to this article can be found online at https://doi.org/10.1016/j.cej.2021.133025.

References

[1] F. Fu, Q. Wang, Removal of heavy metal ions from wastewaters: a review, J Environ Manage 92 (3) (2011) 407–418.

[2] L. Jarup, Hazards of heavy metal contamination, Br Med Bull 68 (2003) 167–182.

[3] Z. Zhao, Z. Liu, H. Wang, W. Dong, W. Wang, Sequential application of Fenton and ozone-based oxidation process for the abatement of Ni-EDTA containing nickel plating effluents, Chemosphere 202 (2018) 238–245.

[4] W. Guan, B. Zhang, S. Tian, X. Zhao, The synergism between electro-Fenton and electrocoagulation process to remove Cu-EDTA, Appl. Catal. B 227 (2018) 252–257.

[5] X. Huang, B. Xie, X. Li, B. Pan, S. Yuan, Y. Zhang, C. Shan, Enhanced HO production from ozonation activated by EDTA, Chem. Eng. J. 288 (2016) 562–568.

[6] C.K. Schmidt, M. Fleig, F. Sacher, H.J. Brauch, Occurrence of aminopolycarboxylates in the aquatic environment of Germany, Environ Pollut 131 (1) (2004) 107–124.

[7] Y. Zhu, W. Fan, T. Zhou, X. Li, Removal of chelated heavy metals from aqueous solution: A review of current methods and mechanisms, Sci Total Environ 678 (2019) 253–266.

[8] S. Liang, X. Hu, H. Xu, Z. Lei, C. Wei, C. Feng, Mechanistic insight into the reaction pathway of peroxomonosulfate-initiated decomplexation of EDTA-NiII under alkaline conditions: Formation of high-valent Ni intermediate, Appl. Catal. B 296 (2021).

[9] L. Song, R. Zhao, D. Yun, P. Lu, J. He, X. Wang, Influence of Co(II), Ni(II), tartrate, and ethylenediaminetetraacetic acid on Cu(II) adsorption onto a polyvinylidene fluoride-based chelating membrane, Toxicol. Environ. Chem. 96 (3) (2014) 362–378.

[10] R.K. Misra, S.K. Jain, P.K. Khatri, Iminodiacetic acid functionalized cation exchange resin for adsorptive removal of Cr(VI), Cd(II), Ni(II) and Pb(II) from their aqueous solutions, J Hazard Mater 185 (2–3) (2011) 1508–1512.

[11] S. Tangtubtim, S. Saikrasun, Effective removals of copper (II) and lead (II) cations from aqueous solutions by polyethyleneimine-immobilized pineapple fiber, Bioresource Technol. Reports 7 (2019).

[12] F. Fu, L. Xie, B. Tang, Q. Wang, S. Jiang, Application of a novel strategy—Advanced Fenton-chemical precipitation to the treatment of strong stability chelated heavy metal containing wastewater, Chem. Eng. J. 189–190 (2012) 283–287.

[13] H. Zeng, S. Liu, B. Chai, D. Cao, Y. Wang, X. Zhao, Enhanced photoelectrocatalytic decomplexation of cu-edta and cu recovery by persulfate activated by uv and cathodic reduction, Environ Sci Technol 50 (12) (2016) 6459–6466.

[14] X. Huang, Y. Xu, C. Shan, X. Li, W. Zhang, B. Pan, Coupled Cu(II)-EDTA degradation and Cu(II) removal from acidic wastewater by ozonation: Performance, products and pathways, Chem. Eng. J. 299 (2016) 23–29.

[15] M.K. Nguyen, V.S. Tran, T.T. Pham, H.G. Pham, B.L. Hoang, T.H. Nguyen, T. H. Nguyen, T.H. Tran, H.H. Ngo, Fenton/ozone-based oxidation and coagulation processes for removing metals (Cu, Ni)-EDTA from plating wastewater, J. Water Process Eng. 39 (2021).

[16] Z. Xu, G. Gao, B. Pan, W. Zhang, L. Lv, A new combined process for efficient removal of Cu(II) organic complexes from wastewater: Fe(III) displacement/UV degradation/alkaline precipitation, Water Res 87 (2015) 378–384.

[17] Z. Xu, C. Shan, B. Xie, Y. Liu, B. Pan, Decomplexation of Cu(II)-EDTA by UV/persulfate and UV/H_2O_2: Efficiency and mechanism, Appl. Catal. B 200 (2017) 439–447.

[18] H. Zhang, N. Li, Y. Wang, D. Zhao, J. He, H. You, J. Jiang, Real-time monitoring of the degradation of Cu(II)-EDTA in H_2O_2/UV using illumination-assisted droplet spray ionization mass spectrometry, Chemosphere 184 (2017) 932–938.

[19] H. Sun, C. Kwan, A. Suvorova, H.M. Ang, M.O. Tadé, S. Wang, Catalytic oxidation of organic pollutants on pristine and surface nitrogen-modified carbon nanotubes with sulfate radicals, Appl. Catal. B 154–155 (2014) 134–141.

[20] C. Cai, H. Zhang, X. Zhong, L. Hou, Ultrasound enhanced heterogeneous activation of peroxymonosulfate by a bimetallic Fe-Co/SBA-15 catalyst for the degradation of Orange II in water, J Hazard Mater 283 (2015) 70–79.

[21] F. Miao, Z. Liu, X. Kang, C. Cheng, X. Mao, R. Li, H. Lin, H. Zhang, Electro-enhanced heterogeneous activation of peroxymonosulfate via acceleration of Fe (III)/Fe(II) redox cycle on Fe-B catalyst, Electrochim. Acta 377 (2021).

[22] Z. Guo, G. Bai, B. Huang, N. Cai, P. Guo, L. Chen, Preparation and application of a novel biochar-supported red mud catalystActive sites and catalytic mechanism, J Hazard Mater 408 (2021), 124802.

[23] X. Lin, K. Shih, J. Chen, X. Xie, Y. Zhang, Y. Chen, Z. Chen, Y. Li, Insight into flower-like greigite-based peroxydisulfate activation for effective bisphenol a abatement: Performance and electron transfer mechanism, Chem. Eng. J. 391 (2020).

[24] A. Ghauch, A.M. Tuqan, Oxidation of bisoprolol in heated persulfate/H_2O systems: Kinetics and products, Chem. Eng. J. 183 (2012) 162–171.

[25] A. Ghauch, A.M. Tuqan, N. Kibbi, Ibuprofen removal by heated persulfate in aqueous solution: A kinetics study, Chem. Eng. J. 197 (2012) 483–492.

[26] A. Ghauch, A.M. Tuqan, N. Kibbi, Naproxen abatement by thermally activated persulfate in aqueous systems, Chem. Eng. J. 279 (2015) 861–873.

[27] A. Ghauch, A. Baalbaki, M. Amasha, R. El Asmar, O. Tantawi, Contribution of persulfate in UV-254 nm activated systems for complete degradation of chloramphenicol antibiotic in water, Chem. Eng. J. 317 (2017) 1012–1025.

[28] S. Al Hakim, S. Jaber, N. Zein Eddine, A. Baalbaki, A. Ghauch, Degradation of theophylline in a UV_{254}/PS system: Matrix effect and application to a factory effluent, Chem. Eng. J. 380 (2020).

[29] A. Ghauch, G. Ayoub, S. Naim, Degradation of sulfamethoxazole by persulfate assisted micrometric Fe^0 in aqueous solution, Chem. Eng. J. 228 (2013) 1168–1181.

[30] G. Ayoub, A. Ghauch, Assessment of bimetallic and trimetallic iron-based systems for persulfate activation: Application to sulfamethoxazole degradation, Chem. Eng. J. 256 (2014) 280–292.

[31] S. Naim, A. Ghauch, Ranitidine abatement in chemically activated persulfate systems: Assessment of industrial iron waste for sustainable applications, Chem. Eng. J. 288 (2016) 276–288.

[32] R. El Asmar, A. Baalbaki, Z. Abou Khalil, S. Naim, A. Bejjani, A. Ghauch, Iron-based metal organic framework MIL-88-A for the degradation of naproxen in water through persulfate activation, Chem. Eng. J. 405 (2021).

[33] D. Huang, G. Zhang, J. Yi, M. Cheng, C. Lai, P. Xu, C. Zhang, Y. Liu, C. Zhou, W. Xue, R. Wang, Z. Li, S. Chen, Progress and challenges of metal-organic frameworks-based materials for SR-AOPs applications in water treatment, Chemosphere 263 (2021), 127672.

[34] S.T. Meek, J.A. Greathouse, M.D. Allendorf, Metal-organic frameworks: a rapidly growing class of versatile nanoporous materials, Adv Mater 23 (2) (2011) 249–267.

[35] M. Pu, Z. Guan, Y. Ma, J. Wan, Y. Wang, M.L. Brusseau, H. Chi, Synthesis of iron-based metal-organic framework MIL-53 as an efficient catalyst to activate persulfate for the degradation of Orange G in aqueous solution, Appl Catal A Gen 549 (2018) 82–92.

[36] X. Li, W. Guo, Z. Liu, R. Wang, H. Liu, Fe-based MOFs for efficient adsorption and degradation of acid orange 7 in aqueous solution via persulfate activation, Appl. Surf. Sci. 369 (2016) 130–136.

[37] T. Yang, D. Yu, D. Wang, T. Yang, Z. Li, M. Wu, M. Petru, J. Crittenden, Accelerating Fe(III)/Fe(II) cycle via Fe(II) substitution for enhancing Fenton-like performance of Fe-MOFs, Appl. Catal. B 286 (2021).

[38] K.-Y. Andrew Lin, H.-A. Chang, C.-J. Hsu, Iron-based metal organic framework, MIL-88A, as a heterogeneous persulfate catalyst for decolorization of Rhodamine B in water. RSC, Advances 5 (41) (2015) 32520–32530.

[39] K. Govindan, M. Raja, M. Noel, E.J. James, Degradation of pentachlorophenol by hydroxyl radicals and sulfate radicals using electrochemical activation of peroxomonosulfate, peroxodisulfate and hydrogen peroxide, J Hazard Mater 272 (2014) 42–51.

[40] P.V. Nidheesh, R. Gandhimathi, Trends in electro-Fenton process for water and wastewater treatment: An overview, Desalination 299 (2012) 1–15.

[41] H. Chi, J. Wan, Y. Ma, Y. Wang, S. Ding, X. Li, Ferrous metal-organic frameworks with stronger coordinatively unsaturated metal sites for persulfate activation to effectively degrade dibutyl phthalate in wastewater, J Hazard Mater 377 (2019) 163–171.

[42] S. Kumar, S. Jain, M. Nehra, N. Dilbaghi, G. Marrazza, K.-H. Kim, Green synthesis of metal–organic frameworks: A state-of-the-art review of potential environmental and medical applications, Coord. Chem. Rev. 420 (2020).

[43] V.I. Isaevaa, L.M. Kustova, b. Microwave activation as an alternative production of metalorganic frameworks, Russ. Chem. Bull. 65 (9) (2016) 2103–2114.

[44] Y. Wan, J. Wan, J.R. Zhao, Y. Wang, T. Luo, S. Yang, Y. Liu, Facile preparation of iron oxide doped Fe-MOFs-MW as robust peroxydisulfate catalyst for emerging pollutants degradation, Chemosphere 254 (2020), 126798.

[45] A. Baalbaki, N. Zein Eddine, S. Jaber, M. Amasha, A. Ghauch, Rapid quantification of persulfate in aqueous systems using a modified HPLC unit, Talanta 178 (2018) 237–245.

[46] Y. Hu, X. Peng, Z. Ai, F. Jia, L. Zhang, Liquid nitrogen activation of zero-valent iron and its enhanced cr(vi) removal performance, Environ Sci Technol 53 (14) (2019) 8333–8341.

[47] G. Song, Z. Wang, L. Wang, G. Li, M. Huang, F. Yin, Preparation of MOF(Fe) and its catalytic activity for oxygen reduction reaction in an alkaline electrolyte, Chin. J. Catal. 35 (2) (2014) 185–195.

[48] Millange, F., Guillou, N., Walton, R.I., Greneche, J.M., Margiolaki, I. and Ferey, G. Effect of the nature of the metal on the breathing steps in MOFs with dynamic frameworks. Chem Commun (Camb) (39), (2008) 4732-4734.

[49] T. Araya, M. Jia, J. Yang, P. Zhao, K. Cai, W. Ma, Y. Huang, Resin modified MIL-53 (Fe) MOF for improvement of photocatalytic performance, Appl. Catal. B 203 (2017) 768–777.

[50] F. Wei, D. Chen, Z. Liang, S. Zhao, Comparison study on the adsorption capacity of rhodamine b, congo red, and orange ii on fe-mofs, Nanomaterials (Basel) 8 (4) (2018).

[51] L. Ai, C. Zhang, L. Li, J. Jiang, Iron terephthalate metal–organic framework: Revealing the effective activation of hydrogen peroxide for the degradation of organic dye under visible light irradiation, Appl. Catal. B 148–149 (2014) 191–200.

[52] Horcajada, P., Serre, C. , Maurin, G. , Ramsahye, N. A. , Balas, F. , & Vallet-Regi, M. , et al. Flexible Porous Metal-Organic Frameworks for a Controlled Drug Delivery. Journal of the American Chemical Society 6774 9 J. AM. CHEM. SOC. 2008, 130, 6774–6780(130.21(2008)), (2008) 6774-6780.

[53] L. Ai, L. Li, C. Zhang, J. Fu, J. Jiang, MIL-53(Fe): a metal-organic framework with intrinsic peroxidase-like catalytic activity for colorimetric biosensing, Chemistry 19 (45) (2013) 15105–15108.

[54] Y. Wan, J. Wan, Y. Ma, Y. Wang, T. Luo, Sustainable synthesis of modulated Fe-MOFs with enhanced catalyst performance for persulfate to degrade organic pollutants, Sci Total Environ 701 (2020), 134806.

[55] T.A. Vu, G.H. Le, C.D. Dao, L.Q. Dang, K.T. Nguyen, Q.K. Nguyen, P.T. Dang, H.T. K. Tran, Q.T. Duong, T.V. Nguyen, G.D. Lee, Arsenic removal from aqueous solutions by adsorption using novel MIL-53(Fe) as a highly efficient adsorbent, RSC Adv. 5 (7) (2015) 5261–5268.

[56] Published J.X.L.N.X. Gao BOPUFENXI (Chinese) 2013 Science Press Place.

[57] Viewer, A.S. Aldrich Spectral Viewer.

[58] X. Liu, Y. Zhou, J. Zhang, L. Tang, L. Luo, G. Zeng, Iron containing metal-organic frameworks: structure, synthesis, and applications in environmental remediation, ACS Appl Mater Interfaces 9 (24) (2017) 20255–20275.

[59] Y. Ou, L. Yao, Y. Li, C. Bai, R. Luque, G. Peng, Magnetically separable Fe-MIL-88B_NH2 carbonaceous nanocomposites for efficient removal of sulfamethoxazole from aqueous solutions, J Colloid Interface Sci 570 (2020) 163–172.

[60] Z.H. Diao, F.X. Dong, L. Yan, Z.L. Chen, W. Qian, L.J. Kong, Z.W. Zhang, T. Zhang, X.Q. Tao, J.J. Du, D. Jiang, W. Chu, Synergistic oxidation of Bisphenol A in a heterogeneous ultrasound-enhanced sludge biochar catalyst/persulfate process: Reactivity and mechanism, J Hazard Mater 384 (2020), 121385.

[61] W. Zheng, L. Zhu, S. Liang, J. Ye, X. Yang, Z. Lei, Z. Yan, Y. Li, C. Wei, C. Feng, Discovering the importance of clo(*) in a coupled electrochemical system for the simultaneous removal of carbon and nitrogen from secondary coking wastewater effluent, Environ Sci Technol 54 (14) (2020) 9015–9024.

[62] L. Xiong, W. Ren, H. Lin, H. Zhang, Efficient removal of bisphenol A with activation of peroxydisulfate via electrochemically assisted Fe(III)-nitrilotriacetic acid system under neutral condition, J Hazard Mater 403 (2021), 123874.

[63] H. Lin, H. Zhang, L. Hou, Degradation of C. I. Acid Orange 7 in aqueous solution by a novel electro/Fe_3O_4/PDS process, J Hazard Mater 276 (2014) 182–191.

[64] Z. Liu, B. Ren, H. Ding, H. He, H. Deng, C. Zhao, P. Wang, D.D. Dionysiou, Simultaneous regeneration of cathodic activated carbon fiber and mineralization of desorbed contaminations by electro-peroxydisulfate process: Advantages and limitations, Water Res. 171 (2020).

[65] Z.-H. Diao, Q. Wei, P.-R. Guo, L.-J. Kong, S.-Y. Pu, Photo-assisted degradation of bisphenol A by a novel $FeS_2@SiO_2$ microspheres activated persulphate process: Synergistic effect, pathway and mechanism, Chem. Eng. J. 349 (2018) 683–693.

[66] Q. Wang, Y. Zhang, Y. Li, J. Ren, G. Qu, T. Wang, H. Jia, Simultaneous Cu-EDTA oxidation decomplexation and Cr(VI) reduction in water by persulfate/formate system: Reaction process and mechanisms, Chem. Eng. J. 427 (2022).

[67] Y. Liu, G. Qu, Q. Sun, H. Jia, T. Wang, L. Zhu, Endogenously activated persulfate by non-thermal plasma for Cu(II)-EDTA decomplexation: Synergistic effect and mechanisms, Chem. Eng. J. 406 (2021).

[68] Z. Xu, T. Wu, Y. Cao, C. Chen, S. Ke, X. Zeng, P. Lin, Efficient decomplexation of heavy metal-EDTA complexes by Co^{2+}/peroxymonosulfate process: The critical role of replacement mechanism, Chem. Eng. J. 392 (2020).

[69] C. Cai, Z. Zhang, H. Zhang, Electro-assisted heterogeneous activation of persulfate by Fe/SBA-15 for the degradation of Orange II, J Hazard Mater 313 (2016) 209–218.

[70] C. Cai, L. Wang, H. Gao, L. Hou, H. Zhang, Ultrasound enhanced heterogeneous activation of peroxydisulfate by bimetallic Fe-Co/GAC catalyst for the degradation of Acid Orange 7 in water, J. Environ. Sci. 26 (6) (2014) 1267–1273.

[71] C. Cai, H. Zhang, X. Zhong, L. Hou, Electrochemical enhanced heterogeneous activation of peroxydisulfate by Fe-Co/SBA-15 catalyst for the degradation of Orange II in water, Water Res 66 (2014) 473–485.

[72] T. Guo, C. Dang, S. Tian, Y. Wang, D. Cao, Y. Gong, S. Zhao, R. Mao, B. Yang, X. Zhao, Persulfate enhanced photoelectrocatalytic degradation of cyanide using a $CuFe_2O_4$ modified graphite felt cathode, Chem. Eng. J. 347 (2018) 535–542.

[73] F. Ghanbari, M. Moradi, Application of peroxymonosulfate and its activation methods for degradation of environmental organic pollutants: Review, Chem. Eng. J. 310 (2017) 41–62.

[74] F. Ji, C. Li, L. Deng, Performance of CuO/Oxone system: Heterogeneous catalytic oxidation of phenol at ambient conditions, Chem. Eng. J. 178 (2011) 239–243.

[75] Z. Huang, Q. Lin, H. Luo, P. Guo, Q. Weng, Y. Lei, S. Cheng, S.-S. Liu, Degradation of progesterone by coexisting free radical and nonradical pathways in the CuO/HNTs-PS system, Chem. Eng. J. 398 (2020).

[76] L. Lyu, L. Zhang, C. Hu, Enhanced Fenton-like degradation of pharmaceuticals over framework copper species in copper-doped mesoporous silica microspheres, Chem. Eng. J. 274 (2015) 298–306.

[77] H. Wang, L. Zhang, C. Hu, X. Wang, L. Lyu, G. Sheng, Enhanced degradation of organic pollutants over Cu-doped $LaAlO_3$ perovskite through heterogeneous Fenton-like reactions, Chem. Eng. J. 332 (2018) 572–581.

[78] M.-Y. Lee, W.-L. Wang, Y. Du, H.-Y. Hu, N. Huang, Z.-B. Xu, Q.-Y. Wu, B. Ye, Enhancement effect among a UV, persulfate, and copper (UV/PS/Cu^{2+}) system on the degradation of nonoxidizing biocide: The kinetics, radical species, and degradation pathway, Chem. Eng. J. 382 (2020).

[79] A. Idrees, A. Shan, M. Ali, Z. Abbas, T. Shahzad, S. Hussain, F. Mahmood, U. Farooq, M. Danish, S. Lyu, Highly efficient degradation of trichloroethylene in groundwater based on persulfate activation by polyvinylpyrrolidone functionalized Fe/Cu bimetallic nanoparticles, J. Environ. Chem. Eng. 9 (4) (2021).

[80] Y. Liu, H. Bai, Q. Zhang, Y. Bai, X. Pang, F. Wang, Y. Yang, J. Ding, W. Fan, W. Shi, In-situ decoration of unsaturated Cu sites on Cu_2O photocathode for boosting nitrogen reduction reaction, Chem. Eng. J. 413 (2021).

[81] H. Zhou, J. Luo, Y. Chen, Nitrogen moieties -dominated Co-N-doped nanoparticle-modified cathodes in heterogeneous-electro-Fenton-like system for catalytic decontamination of EDTA-Ni(II), Chemosphere 239 (2020), 124743.

[82] S. Lan, Y. Xiong, S. Tian, J. Feng, T. Xie, Enhanced self-catalytic degradation of CuEDTA in the presence of H_2O_2/UV: Evidence and importance of Cu-peroxide as a photo-active intermediate, Appl. Catal. B 183 (2016) 371–376.

[83] Y. Liu, D. Wang, M. Xue, R. Song, Y. Zhang, G. Qu, T. Wang, High-efficient decomplexation of Cu-EDTA and Cu removal by high-frequency non-thermal plasma oxidation/alkaline precipitation, Sep. Purif. Technol. 257 (2021).

[84] Z. Liu, C. Zhao, P. Wang, H. Zheng, Y. Sun, D.D. Dionysiou, Removal of carbamazepine in water by electro-activated carbon fiber-peroxydisulfate: Comparison, optimization, recycle, and mechanism study, Chem. Eng. J. 343 (2018) 28–36.

[85] H. Yoshioka, Y. Senba, K. Saito, T. Kimura, F. Hayakawa, Spin-trapping study on the hydroxyl radical formed from a tea catechin-Cu(II) system, Biosci Biotechnol Biochem 65 (8) (2001) 1697–1706.

[86] C. Zhu, G. Fang, D.D. Dionysiou, C. Liu, J. Gao, W. Qin, D. Zhou, Efficient transformation of DDTs with Persulfate Activation by Zero-valent Iron Nanoparticles: A Mechanistic Study, J Hazard Mater 316 (2016) 232–241.

[87] H. Ding, Y. Zhu, Y. Wu, J. Zhang, H. Deng, H. Zheng, Z. Liu, C. Zhao, In situ regeneration of phenol-saturated activated carbon fiber by an electro-peroxymonosulfate process, Environ Sci Technol 54 (17) (2020) 10944–10953.

[88] J.J. Pignatello, E. Oliveros, A. MacKay, Advanced oxidation processes for organic contaminant destruction based on the fenton reaction and related chemistry, Critical Review. Environ. Sci. Technol. 36 (1) (2006) 1–84.

[89] Enric Brillas I.S.s. A. Mehmet Oturan* electro-fenton process and related electrochemical technologies based on fenton's reaction chemistry Chem. Rev. 10/19/2009, (2009).